Empirical Relations between Size Parameters of Ice Hydrometeor Populations and Radar Reflectivity

SERGEY Y. MATROSOV

Cooperative Institute for Research in Environmental Sciences, University of Colorado Boulder, and NOAA/Earth System Research Laboratory, Boulder, Colorado

ANDREW J. HEYMSFIELD

National Center for Atmospheric Research,[a] *Boulder, Colorado*

(Manuscript received 22 March 2017, in final form 29 June 2017)

ABSTRACT

Empirical power-law relations between the equivalent radar reflectivity factor Z_e and the slope parameter of the gamma function Λ (i.e., $\Lambda = cZ_e^d$; used to describe ice hydrometeor size distributions) are derived. The Λ parameter can also be considered as a size parameter since it is proportional to the inverse of the hydrometeor characteristic size, which is an important geophysical parameter describing the entire distribution. Two datasets from two-dimensional microphysical probes, collected during aircraft flights in subtropical and midlatitude regions, were used to obtain Λ by fitting measured size distributions. Reflectivity for different radar frequencies was calculated from microphysical probe data by using nonspherical-particle models. The derived relations have exponent d values that are approximately from -0.35 to -0.40, and the prefactors c are approximately between 30 and 55 (Λ: cm^{-1}; Z_e: $\mathrm{mm}^6\,\mathrm{m}^{-3}$). There is a tendency for d and c to decrease when radar frequency increases from K_u band (~14 GHz) to W band (~94 GHz). Correlation coefficients between Z_e and Λ can be very high (~0.8), especially for lower frequencies. Such correlations are similar to those for empirical relations between reflectivity and ice water content (IWC), which are used in many modeling and remote sensing applications. Close correspondences of reflectivity to both Λ and IWC are due to a relatively high correlation between these two microphysical parameters. Expected uncertainties in estimating Λ from reflectivity could be as high as a factor of 2, although estimates at lower radar frequencies are more robust. Stratifying retrievals by temperature could result in relatively modest improvement of Λ estimates.

1. Introduction

Empirical relations between the equivalent radar reflectivity factor (hereinafter just reflectivity) Z_e and cloud/precipitation ice water content (IWC) have been long used in different remote sensing and model applications. Such relations are typically sought in a power-law form

$$\mathrm{IWC} = aZ_e^b, \tag{1}$$

where empirically derived values of the exponent b are usually between 0.4 and 0.7 for radar frequencies below ~36 GHz (when Z_e is in linear units: $\mathrm{mm}^6\,\mathrm{m}^{-3}$), and the prefactor coefficient a varies over a much wider range. Sometimes a is considered to be temperature dependent (e.g., Hogan et al. 2006). Even though multisensor retrievals (e.g., Shupe et al. 2016) or retrievals that use multiple radar variables (e.g., Matrosov et al. 2002; Maahn and Loehnert 2017) are potentially more accurate, the utility of empirical relations such as Eq. (1) is still important in many practical situations in which only radar reflectivity measurements are available (e.g., when observing optically thick ice clouds with spaceborne radars; Matrosov and Heymsfield 2008).

The most common approach for deriving empirical IWC–Z_e relations is performing a regression between calculated or directly measured bulk IWC (e.g., Heymsfield et al. 2016) and reflectivity values calculated from in situ cloud/precipitation two-dimensional (2D) microphysical-probe particle size distributions (PSDs). The reflectivity values are calculated by using some

[a] The National Center for Atmospheric Research is sponsored by the National Science Foundation.

Corresponding author: Sergey Y. Matrosov, sergey.matrosov@noaa.gov

DOI: 10.1175/JAMC-D-17-0076.1

theoretical model that assumes particle shapes and size-dependent masses. On rare occasions, actual radar reflectivity measurements are coordinated with in situ microphysical measurements so that the corresponding relations can be drawn from independent sets of data. Such relations, however, are often within the variability range of relations derived using the common approach (e.g., Protat et al. 2016).

The correspondence between IWC and Z_e depends on the details of the PSD. One of the most important PSD parameters is the size parameter that characterizes particle sizes in some mean sense. Variability of this parameter influences the data spread in the IWC–Z_e relations and thus affects the reflectivity-based retrieval errors of IWC. The size parameter is also an important geophysical variable that is usually considered as a retrieval unknown when applying relations such as Eq. (1). There is, however, a significant correlation between the characteristic sizes of ice-particle populations (e.g., mean, median, or effective sizes) and radar reflectivity (e.g., Matrosov 1997).

The objectives of this study include evaluations of mean correspondences between radar reflectivity and different PSD parameters, emphasizing one that describes the characteristic particle size, which represents the entire distribution, assessing a degree of correlation between Z_e and different PSD parameters, and comparing it with that between Z_e and IWC. The correspondences between the size parameter and reflectivity expressed as empirical power-law relations in a way that is similar to IWC–Z_e relations can be potentially used for practical applications, including remote sensing of ice microphysical parameters. Interrelations between the size parameter and IWC are also evaluated. These interrelations are responsible, in part, for correspondences of these microphysical parameters to reflectivity.

2. Correspondences between reflectivity and PSD parameters

Experimentally measured PSDs are often fitted by analytical functional forms because such forms are convenient for modeling studies and remote sensing applications. The most common form is the one that describes the particle concentrations N by the gamma function in terms of the major particle dimensions D as inferred from 2D in situ microphysical probes (e.g., Kosarev and Mazin 1991):

$$N = N_0 D^{\mu} \exp(-\Lambda D), \tag{2}$$

where N_0, μ, and Λ are the intercept, the dispersion (width) parameter, and the distribution slope, respectively. Slope Λ can also be considered as the PSD size parameter, which describes the characteristic particle size of the entire size distribution, because it is proportional to the inverse of median volume particle size $D_{\rm mv}$. For nontruncated gamma-function distributions assuming similarity of shapes of particles of different sizes (e.g., Bringi and Chandrasekar 2001):

$$\Lambda \approx (3.67 + \mu)/D_{\rm mv}. \tag{3}$$

Exponential size distributions, which are often used in practice, are a special case of the gamma-function PSDs when $\mu = 0$. Field et al. (2007) showed that exponential distributions often provide a good approximation for higher PSD moments.

Given that Λ is a microphysical parameter that is useful for many model and remote sensing applications, it is instructive to assess whether practical power-law relations of the type that are used to derive IWC from radar reflectivity measurements can be suggested for estimations of Λ, that is,

$$\Lambda = cZ_e^d. \tag{4}$$

Figures 1a and 1b show scatterplots of the gamma-function slope parameter Λ versus the K_a-band (~35 GHz) radar reflectivity ($Z_e > -20$ dBZ) as derived from microphysical in situ datasets obtained during two aircraft-measurement field experiments that were conducted in different environments. Procedures for deriving Λ, μ, and N_0 from experimental PSDs are described by Heymsfield et al. (2002). The K_a-band frequencies are the most common operational frequencies of cloud radars, and they are utilized in many ground-based radars worldwide, including those at different facilities (e.g., Southern Great Plains in Oklahoma, Barrow and Oliktok Point in Alaska, and Azores) of the U.S. Department of Energy Atmospheric Radiation Measurement program (Mather and Voyles 2013) and more recently in radar observations from space (Hou et al. 2014).

The microphysical sample data for this study come from the Global Precipitation Measurement (GPM) Cold Season Precipitation Experiment (GCPEX), which was conducted in Canada during January–February of 2012 (Skofronick-Jackson et al. 2015), and the Cirrus Regional Study of Tropical Anvils and Cirrus Layers–Florida-Area Cirrus Experiment (CRYSTAL-FACE), which was conducted in the summer of 2002 (Heymsfield et al. 2005). The GCPEX observations were primarily from stratiform ice- and mixed-phase clouds (including precipitating clouds), although some lake-effect snowbands were sampled. The CRYSTAL-FACE data were primarily from summertime ice clouds associated with convective cloud outflow. The GCPEX data were collected at generally

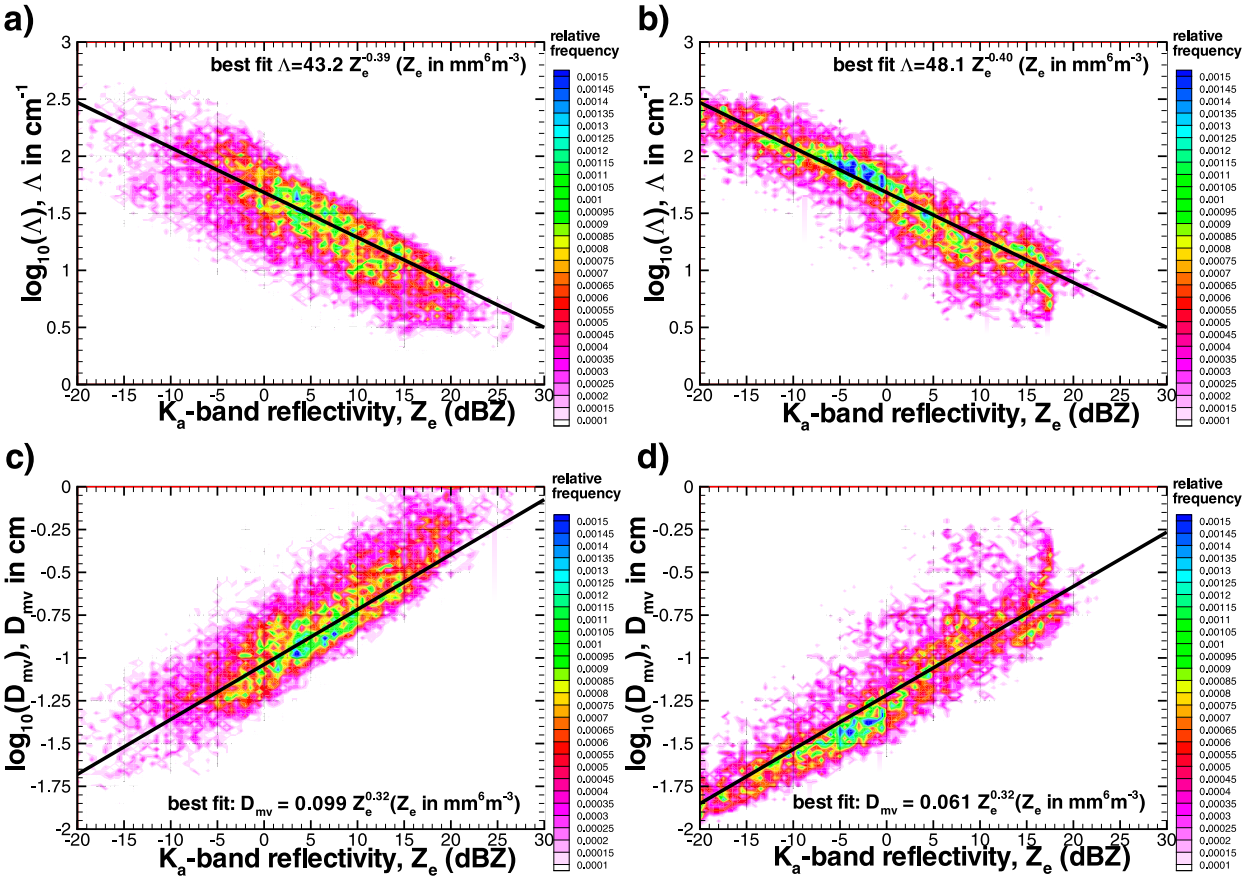

FIG. 1. Scatterplots of K_a-band radar reflectivity vs (a),(b) the PSD slope parameter Λ and (c),(d) median volume particle size as derived from the (left) GCPEX and (right) CRYSTAL-FACE microphysical data.

warmer temperatures than were the CRYSTAL-FACE data (average ambient air temperatures were approximately −14° and −33°C for these datasets, respectively). There are 17 773 and 11 478 samples in the Fig. 1 GCPEX and CRYSTAL-FACE scatterplots, respectively.

Two-dimensional particle probes for collecting cloud microphysical information were used in both cases (Heymsfield et al. 2005, 2016). Shattering of large particles on the leading surfaces of 2D microphysical probes can cause artifacts that result in enhanced concentrations of small ice. To alleviate shattering effects, such artifacts were objectively removed on the basis of particle interarrival times and Poisson statistics (Heymsfield et al. 2010).

Radar reflectivity values were calculated using the observed PSDs, estimated ice-particle mass from direct or calculated-from-PSD IWC data, and the **T**-matrix approach for the oblate spheroidal particles oriented on average with their major dimensions in the horizontal plane (Matrosov 2007) and assuming a 10° standard deviation from this preferential orientation (e.g., Matrosov et al. 2005). A zenith/nadir-viewing radar geometry and a particle aspect ratio of 0.6 were assumed. Assumptions of such aspect ratios and small deviations from the preferable horizontal orientations were previously shown to satisfactorily explain dual-wavelength and polarimetric radar measurements of ice hydrometeors (e.g., Hogan et al. 2012; Matrosov 2015).

Calculating radar reflectivity requires an assumption of individual particle mass–size (m–D) relations. These relations are generally presented in a power-law form (i.e., $m = fD^g$). The exponent in these relations is typically close to 2 while the coefficient varies much more (Heymsfield et al. 2013). For the CRYSTAL-FACE dataset, the coefficient f was adjusted on the basis of measurements of the bulk mass from the counterflow virtual impactor (CVI) probe as described by Matrosov and Heymsfield (2008). Direct collocated CVI measurements were not available during the GCPEX campaign. The GCPEX reflectivity and IWC data were derived using the m–D relation ($g = 2.1$; $f = 0.005\,28$ in cgs units; $f = 0.0837$ in SI units) that was found to provide the best agreement between the total mass obtained by integrating PSD data and that from concurrent CVI measurements in a wide range of ice clouds (Heymsfield et al. 2016).

TABLE 1. Prefactor c and exponent d in mean relations of the form of Eq. (4) (Z_e: mm^6 m^{-3}; Λ: cm^{-1}). Also given are the power-law correlation coefficient cc and the NMAD of the power-law approximations.

	GCPEX dataset				CRYSTAL-FACE dataset			
	c	d	cc	NMAD	c	d	cc	NMAD
K_u band	47.1	−0.36	0.85	48%	54.1	−0.36	0.90	34%
K_a band	43.2	−0.39	0.81	51%	48.1	−0.40	0.86	37%
W band	28.1	−0.40	0.60	62%	32.9	−0.42	0.70	49%

As seen from the data in Figs. 1a and 1b and Table 1, there is good correlation between Λ and radar reflectivity. The Λ–Z_e relations for datasets from both field campaigns are relatively close to each other. It is also evident from Figs. 1a and 1b that, on average, Λ values for the GCPEX dataset are smaller than those for CRYSTAL-FACE (mean values are approximately 49 and 74 cm^{-1}, respectively). This indicates generally larger particle populations during the GCPEX flights. Table 1 shows coefficients of the best-fit power-law Λ–Z_e relations at K_a band from Fig. 1 and also for corresponding relations at K_u (~14 GHz) and W (~94 GHz) radar frequencies, which are also common frequencies used in meteorological radars. A K_u-band frequency (in addition to a K_a-band frequency) is used in the dual-wavelength spaceborne GPM radar, and W-band cloud radars are also now increasingly used for ground-based (e.g., Mather and Voyles 2013) and airborne [and also *CloudSat* spaceborne (e.g., Tanelli et al. 2008)] measurements of atmospheric hydrometeors.

Table 1 also presents correlation coefficients and normalized mean absolute difference (NMAD) values of Λ estimates derived from the best-fit relation:

$$\mathrm{NMAD} = \langle |X_o - X_b| \rangle / \langle |X_o| \rangle \times 100\%, \qquad (5)$$

where X_o and X_b are the values of variable X (in this case X is Λ) from the microphysical probes and from the best-fit relations and angle brackets indicate data averaging for a particular dataset. The NMAD values characterize the quality of the best-fit approximation because they describe the data scatter around this approximation. These values can be considered to be a measure of the uncertainty of Λ retrievals if reflectivity is well known. As seen from Table 1, these values generally increase with frequency, which is, in part, due to decreasing sensitivity of reflectivity to particle sizes as a result of effects from non-Rayleigh scattering. Errors in reflectivity measurements and particle models would introduce an additional retrieval uncertainty.

Scattering at K_u-band frequencies is for the most part in the Rayleigh-scattering regime for particles that are smaller than ~3.5 mm. Electromagnetic scattering at W band is essentially non-Rayleigh for particles larger than ~0.5 mm. The spheroidal-shape model has some limitations for calculating backscatter at W band for very large particles (e.g., Leinonen et al. 2012). As shown in Hogan and Westbrook (2014), however, when integrated over the PSD the backscatter differences in the reflectivity from the spheroidal model and that from more sophisticated particle models are often comparable to the differences caused by a reasonable uncertainty in aspect ratios for the same particle-shape model (e.g., 0.5 vs 0.6).

In addition to the Λ and Z_e relations, Figs. 1c and 1d show scatterplots between D_{mv} [as in Eq. (3)] and reflectivity. The corresponding power-law correlation coefficients between these variables are somewhat smaller (i.e., ~0.78–0.80) than those for the Λ and Z_e pair. This is, in part, due to the variability in μ. On average, D_{mv} values for the CRYSTAL-FACE data are substantially smaller than for the GCPEX data, which is, in part, caused by the differences in μ values from these observational datasets. For particle populations with size-dependent bulk density, median mass sizes, which are also used for describing the entire distributions, are generally smaller than D_{mv}. For values of μ between 0 and 1 and the mass–size relation exponent $g \approx 2$, the ratio of median volume and median mass sizes is approximately between 0.73 and 0.78 if D_{mv} is greater than ~0.05 cm (Matrosov et al. 1995).

Although the correlation between Λ and Z_e is relatively high, it is not so for relations between reflectivity and other PSD parameters. Figure 2 shows scatterplots between μ, which is dimensionless, and Z_e. Although there is some trend for μ to diminish when reflectivity increases, the corresponding correlation coefficient is only 0.43 for the GCPEX data and 0.37 for the CRYSTAL-FACE data. Values of μ for both datasets generally vary in a relatively small dynamic range between −2 and 2.

The units of the gamma-function parameter N_0 depend on μ, and this parameter has a very large range of variability, which makes it inconvenient for intercomparisons and characterizing particle size distributions. Often, a normalized intercept parameter of the exponential (i.e., when μ is forced to be 0) distribution is considered for practical applications (e.g., Bringi and Chandrasekar 2001). Parameter $N_0(\mu = 0)$ has units of

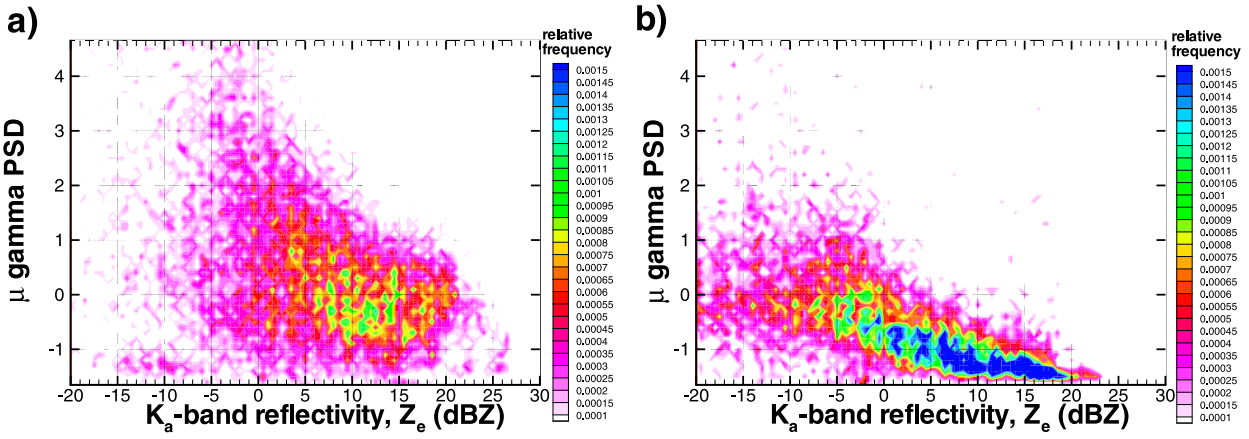

FIG. 2. Scatterplots between the PSD μ parameter and K_a-band radar reflectivity as derived from the (a) GCPEX and (b) CRYSTAL-FACE microphysical data.

length^{-4} and a smaller dynamic range of variability. It is widely used for describing raindrop size distributions. Figure 3 shows scatterplots of $N_0(\mu = 0)$ versus radar reflectivity for the two microphysical datasets that are considered in this study. Power-law correlation coefficients between $N_0(\mu = 0)$ and Z_e are only 0.46 and 0.28 for the GCPEX and CRYSTAL-FACE data, respectively. The $N_0(\mu = 0)$ values are noticeably larger for the CRYSTAL-FACE dataset. Since μ values for this dataset are generally smaller, it indicates larger relative fractions of smaller particles when compared with the GCPEX microphysical samples. This is consistent with generally larger Λ values observed during the CRYSTAL-FACE campaign and is due to the convective nature of the clouds that were sampled.

The GCPEX and CRYSTAL-FACE microphysical data were also used to derive ice water content–reflectivity correspondences, which are shown in Fig. 4. The presented IWC values from CRYSTAL-FACE were derived from the CVI measurements, whereas GCPEX IWC values were calculated using the PSD, as described above. Power-law correlation coefficients between IWC and Z_e are 0.86 and 0.73 for GCPEX and CRYSTAL-FACE measurements, which are comparable to those between Λ and Z_e. The prefactor coefficients in the best-fit power-law IWC–Z_e relations differ considerably between the datasets, even though both fits are within the variability range of such relations derived from different microphysical datasets (e.g., Matrosov 1997; Hogan et al. 2006). The differences in the prefactor values are in part due to the fact that particles were on average larger (as evident from smaller Λ values) during GCPEX flights when compared with those observed during the CRYSTAL-FACE campaign. Larger particle populations result in smaller prefactor values in the power-law IWC–Z_e relations (Atlas et al. 1995).

Overall, it can be concluded from the data presented that correlations between reflectivity and the size parameter and also between reflectivity and IWC are noticeably higher than those between reflectivity and other PSD parameters (i.e., μ and N_0). Thus, radar reflectivity measurements are more promising for estimating Λ and

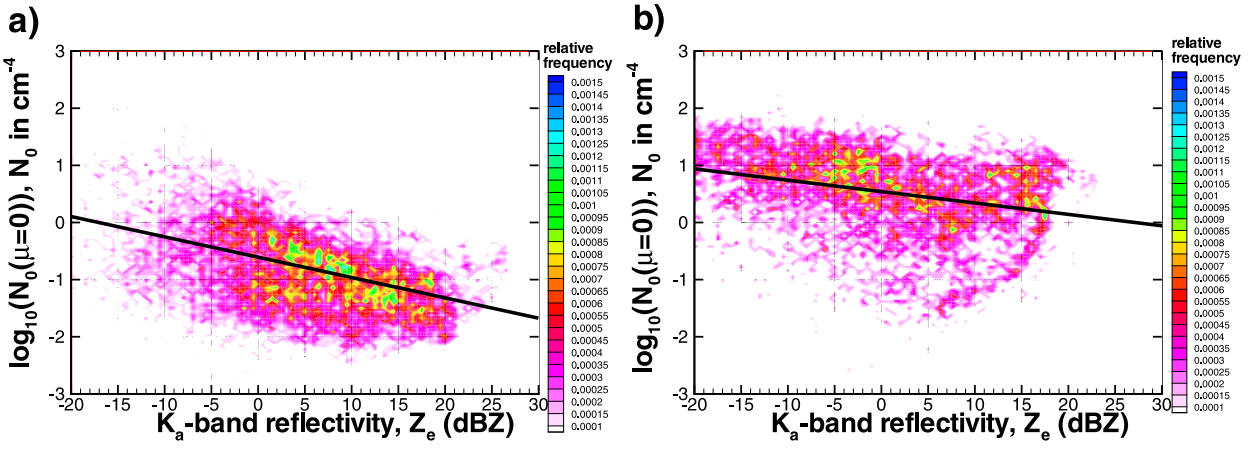

FIG. 3. As in Fig. 2, but for the PSD parameter N_0.

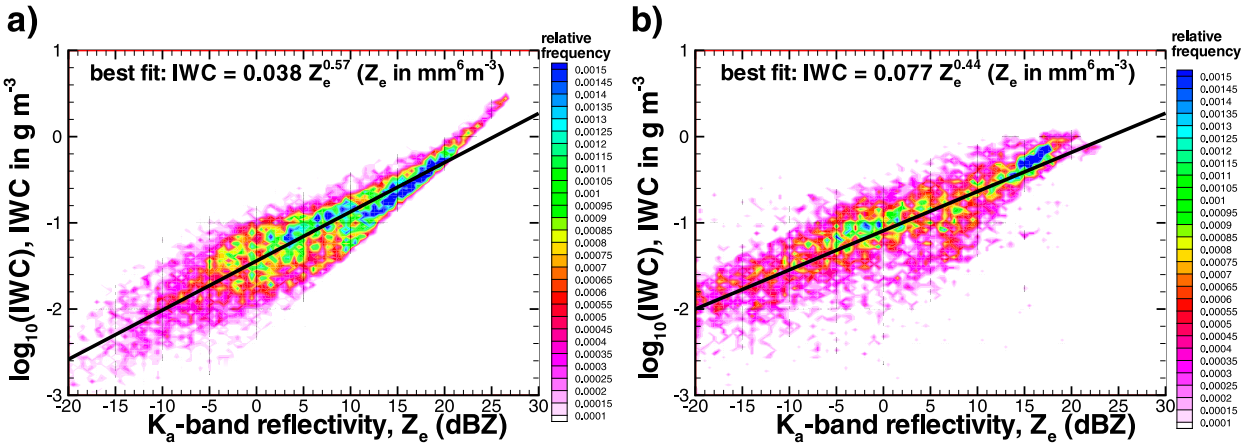

FIG. 4. As in Fig. 2, but for the IWC.

IWC than other PSD characteristics. A relatively high correlation between IWC and Z_e is widely used in many remote sensing and model applications, which is not the case for statistical relations between hydrometeor characteristic size parameter and reflectivity.

3. Consistency of Λ–Z_e and IWC–Z_e relations

The fact that both IWC and Λ are relatively well correlated with radar reflectivity is not surprising because Z_e is a strong function of both the total ice mass and the characteristic particle size of the distribution (e.g., Atlas et al. 1995). There is also a significant interrelation between IWC and Λ as higher values of IWC are typically observed from in situ samples of larger particle populations and at warmer temperatures. This results in the fact that Λ–Z_e and IWC–Z_e empirical relations are generally interdependent.

This interdependency is further illustrated in Fig. 5, which depicts the scatterplots between IWC and Λ from the microphysical in situ measurements. The data-scatter areas are somewhat similar for the both the GCPEX and CRYSTAL-FACE data. The Λ–Z_e and IWC–Z_e best-fit power-law relations for each dataset (Figs. 1a and 4a and Figs. 1b and 4b, respectively) were combined to derive IWC–Λ consistency relations, which are shown in Fig. 5 by gray lines. Also shown in Fig. 5 are best-fit power-law relations (black lines) obtained by directly regressing Λ and IWC estimates from the microphysical probes.

Overall, both the consistency relations and power-law best-fit IWC–Λ relations in Fig. 5 describe the observed correspondence between these two variables well, although the NMAD values for the latter relations (71% and 69% for GCPEX and CRYSTAL-FACE data, respectively) are, as expected, lower than for the former relations (i.e., 90% and 74%, respectively). Deriving two variables (i.e., Λ and IWC) from one Z_e measurement becomes only possible because there is a significant interrelation between these two microphysical variables.

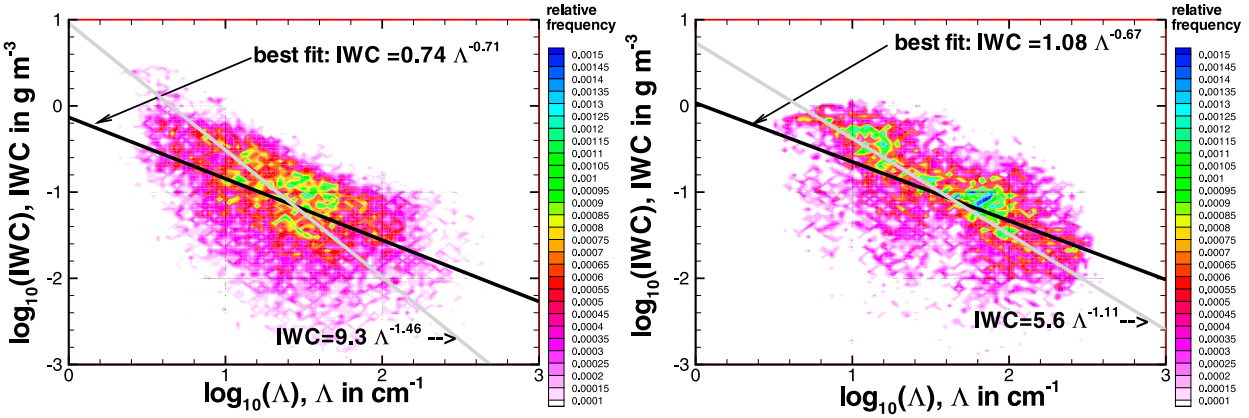

FIG. 5. Correspondence between the PSD slope parameter Λ and IWC (black lines) as inferred from the (a) GCPEX and (b) CRYSTAL-FACE microphysical data. The gray lines show the consistency relations derived by combining the Λ–Z_e and IWC–Z_e best power-law fits.

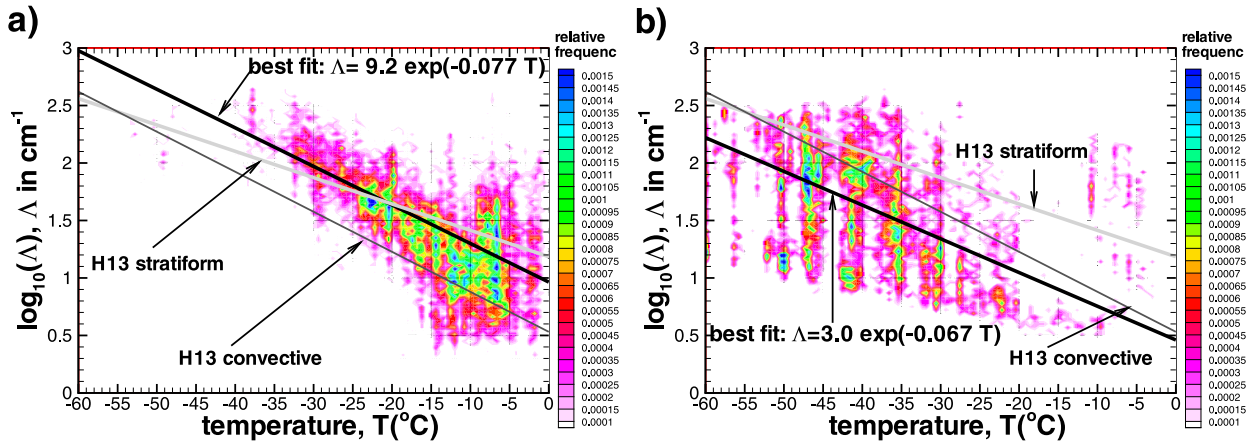

FIG. 6. Scatterplots of the ambient temperature vs the PSD slope parameter Λ as derived from the (a) GCPEX and (b) CRYSTAL-FACE microphysical data. Mean power-law fits from Heymsfield et al. (2013) are also shown.

4. Temperature dependence of Λ–Z_e relations

Figure 6 shows scatterplots between Λ and environmental air temperature T. Comparing Figs. 1 and 4 reveals that the data scatter is considerably less in the Λ–Z_e relations than in the Λ–T relations, even though there are obvious general trends of decreasing Λ (i.e., increasing characteristic particle size of the PSD) with increasing temperature. The NMAD values of the exponential best fits shown in Fig. 6 are around 66% and 72% for the GCPEX and CRYSTAL-FACE datasets, respectively. The temperature trends of Λ in these datasets, however, are somewhat different, with the GCPEX dataset showing a greater sensitivity to temperature and the data scatter for the CRYSTAL-FACE data being particularly wide. It indicates that the temperature only might not be a very robust indicator of characteristic size of particle populations. For reference, mean Λ–temperature trends from a study by Heymsfield et al. (2013) are also shown in Fig. 6.

The temperature influence on the empirical Λ–Z_e relations was further investigated by constructing best power-law fits in several temperature intervals. The corresponding results are shown in Fig. 7. Overall, for the same reflectivity values, progressively smaller particle populations are seen as temperatures become colder. For the CRYSTAL-FACE dataset, differences among Λ–Z_e relations for different temperature intervals are smaller relative to GCPEX samples.

Although the mean Λ–Z_e relations for both datasets are relatively close, it is not generally so when comparing corresponding relations for different temperature intervals. For a particular dataset, applying temperature-dependent Λ–Z_e relations instead of the mean of such a relation results in modest improvement in Λ estimates. For the GCPEX data, NMAD values of temperature-tuned K_a-band reflectivity-based Λ estimates are generally between 35% and 44% as compared with approximately 51% (see Table 1) when the mean relation is used. For

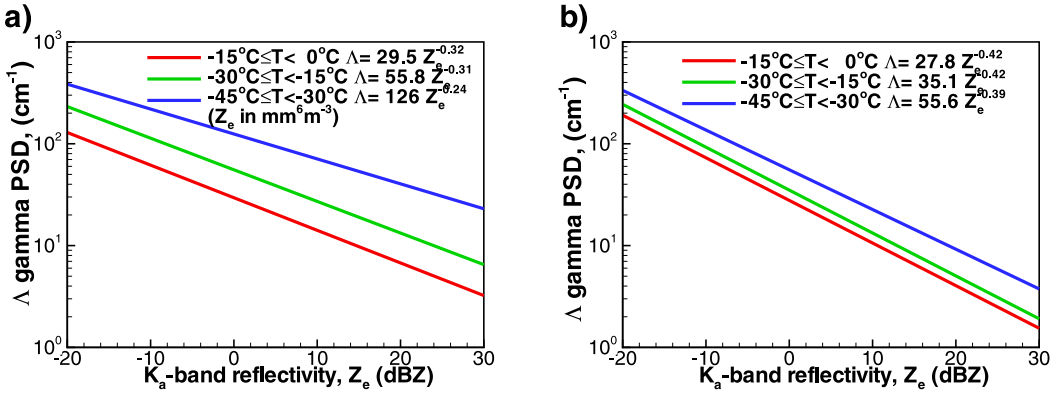

FIG. 7. Best-fit power-law Λ–Z_e K_a-band relations stratified by the temperature intervals for the (a) GCPEX and (b) CRYSTAL-FACE microphysical data.

the CRYSTAL-FACE dataset, the use of temperature-dependent relations instead of the mean one results only in small changes (typically within a few percentage points, in terms of the NMAD). The use of a "wrong" temperature-dependent relation can change estimates of Λ by about 30% or so. Relative changes of NMAD values when using temperature-dependent Λ–Z_e relations for other radar frequencies are similar.

5. Uncertainties of Λ–Z_e relations

NMAD values represent the data scatter around the best-fit relations. This data scatter contributes to the uncertainty of Λ estimates from reflectivity measurements. Other sources of retrieval uncertainties are reflectivity errors, including the uncertainties of the particle model used for calculating reflectivity. An assumed particle aspect ratio and the **T**-matrix spheroidal-approximation approach represent major sources of model uncertainties, which are more pronounced at higher radar frequencies (i.e., W band).

As mentioned in section 2, differences between the spheroidal approximation and more complex particle models at W band are comparable to the differences due to different assumptions about particle aspect ratio (e.g., 0.5 vs 0.6). Note also that actual aspect ratios can be somewhat smaller than those inferred from 2D projected images. Underestimations of W-band reflectivities of particle populations calculated using the spheroidal model and the **T**-matrix approach can be as much as 2 dB or so for higher reflectivities of ~10 dBZ (Hogan and Westbrook 2014). Only about 5% of data points from the GCPEX and CRYSTAL-FACE campaigns, however, result in W-band reflectivities (which are appreciably smaller than lower-frequency reflectivities) of greater than 10 dBZ. Two-dimensional projected images of typical ice particles with most common irregular shapes indicate mean projectional aspect ratios of about 0.6 and corresponding standard deviations of 0.1 or so (Korolev and Isaac 2003). The **T**-matrix modeling (not shown) indicates that a 0.1 aspect-ratio uncertainty would result in approximately 0.5-dB changes in W-band reflectivity for constant mass PSDs with typical average values of $\Lambda = 50\,\mathrm{cm}^{-1}$ and $\mu = 0$.

In addition, an approximately 20% uncertainty in the particle mass–size relation would result in about 1.5-dB errors of calculated reflectivity (Hammonds et al. 2014). Given the aforementioned reflectivity uncertainties due to the particle model and an independence of errors due to the particle model and uncertainties in the m–D relation, a conservative uncertainty value of 3 dB in W-band reflectivities can be assumed. Since a typical exponent in the Λ–Z_e relations is about −0.40, a factor-of-2 (i.e., 3 dB) reflectivity uncertainty would correspond to about 30% uncertainty in Λ. If, further, this 30% uncertainty and the NMAD scatter of ~60% are assumed to be independent, the total Λ error of ~70% can be estimated as a square root of the sum of squares of individual contributions. Errors of estimating Λ at lower radar frequencies are expected to be smaller relative to the W band because of generally lower NMAD values for the corresponding Λ–Z_e relations and smaller uncertainties of the spheroidal-particle reflectivity model.

6. Conclusions

Aircraft-based microphysical sampling data were used to investigate statistical relations between the ice hydrometeor size distribution parameters and radar reflectivity factor Z_e. The datasets were collected during two field campaigns conducted in different environments. The GCPEX campaign was conducted in wintertime clouds and precipitation during flights over Canada, and the CRYSTAL-FACE campaign flights were performed in Florida primarily in summertime high ice layers associated with convective cloud outflow. The datasets included here are large, each containing more than 10 000 in-cloud flight samples. A summary of the results is given here—the aircraft sampling datasets are available from the authors upon request.

A relatively robust correspondence was found between Z_e and an ice hydrometeor size distribution slope parameter Λ, which is proportional to the inverse of the particle characteristic size and describes the entire PSD. The empirical relations between these two parameters were presented using power-law fits. The correlation coefficients between Z_e and Λ were about 0.8 (0.6–0.7 at W band). This is comparable to those for empirical relations between reflectivity and ice water content. The fact that both microphysical parameters (i.e., IWC and Λ) are strongly related to the radar reflectivity is explained by the close correspondence between these two microphysical parameters. In the typical case, larger particle populations are associated with higher ice water contents.

The mean power-law Λ–Z_e relations for the datasets from the GCPEX and CRYSTAL-FACE field projects are relatively close to each other, and the normalized absolute differences that characterize the data scatter around the best-fit approximations are typically between 32% and 60%. The data scatter increases with the radar frequency. For a given microphysical dataset, stratifying these relations on the basis of the ambient air temperature could provide modest improvement, resulting in relatively small changes in NMAD values.

The findings of this study suggest that Λ–Z_e relations can be as robust as IWC–Z_e relations, which are used

extensively in numerous studies ranging from microphysical modeling to remote sensing. Empirical Λ–Z_e relations could also be useful in many practical applications—for example, when inferring the characteristic size of the ice hydrometeors is of particular interest. Since the characteristic size of a distribution can be used to assess the particle ensemble mean density (e.g., Matrosov 2015), such applications can include interpretations of radar polarimetric variables whose dependence on hydrometeor shape is strongly influenced by particle density. Unlike for the Z_e and Λ pair, correlations between radar reflectivity and other PSD parameters for considered datasets were not strong.

Expected uncertainties of estimating the size parameter Λ from radar reflectivity measurements are determined by the data scatter around the best-fit relations and reflectivity uncertainties, including those of the particle model used for calculating reflectivities. With reasonable assumptions for the error contributions noted above, the total estimation uncertainties can be expected to be as high as ~70% on average (or roughly as a factor of 2) for the higher-frequency radar measurements. Estimates at lower radar frequencies might be more robust because there is less influence of non-Rayleigh scattering and smaller sensitivity to particle shapes. More studies of the correspondence between the Λ parameter and radar reflectivity at different frequency bands (including coincident direct measurements of reflectivity) are needed in the future to better understand the variability in PSD size parameter–reflectivity relations.

Acknowledgments. This work was supported in part by National Aeronautics and Space Administration Grants NNX16AQ36G and NNX16AP28G and U.S. Department of Energy Office of Science Atmospheric System Research Program Grant DE-SC0013306.

REFERENCES

Atlas, D., S. Y. Matrosov, A. J. Heymsfield, M. D. Chao, and D. B. Wolff, 1995: Radar and radiation properties of ice clouds. *J. Appl. Meteor.*, **34**, 2329–2345, doi:10.1175/1520-0450(1995)034<2329:RARPOI>2.0.CO;2.

Bringi, V. N., and V. Chandrasekar, 2001: *Polarimetric Doppler Weather Radar.* Cambridge University Press, 636 pp.

Field, P. R., A. J. Heymsfield, and A. Bansemer, 2007: Snow size distribution parameterization for midlatitude and tropical ice clouds. *J. Atmos. Sci.*, **64**, 4346–4365, doi:10.1175/2007JAS2344.1.

Hammonds, K. D., G. G. Mace, and S. Y. Matrosov, 2014: Characterizing the radar backscatter-cross-section sensitivities of ice-phase hydrometeor size distributions via a simple scaling of the Clausius–Mossotti factor. *J. Appl. Meteor. Climatol.*, **53**, 2761–2774, doi:10.1175/JAMC-D-13-0280.1.

Heymsfield, A. J., A. R. Bansemer, P. R. Field, S. L. Durden, J. L. Stith, J. E. Dye, W. D. Hall, and C. A. Grainger, 2002: Observations and parameterizations of particle size distributions in deep tropical cirrus and stratiform precipitating clouds: Results from in situ observations in TRMM field campaigns. *J. Atmos. Sci.*, **59**, 3457–3491, doi:10.1175/1520-0469(2002)059<3457:OAPOPS>2.0.CO;2.

——, Z. Wang, and S. Matrosov, 2005: Improved radar ice water content retrieval algorithms using coincident microphysical and radar measurements. *J. Appl. Meteor.*, **44**, 1391–1412, doi:10.1175/JAM2282.1.

——, C. Schmitt, A. Bansemer, and C. H. Twohy, 2010: Improved representation of ice particle masses based on observations in natural clouds. *J. Atmos. Sci.*, **67**, 3303–3318, doi:10.1175/2010JAS3507.1.

——, ——, and ——, 2013: Ice cloud particle size distributions and pressure-dependent terminal velocities from in situ observations at temperatures from 0° to −86°C. *J. Atmos. Sci.*, **70**, 4123–4154, doi:10.1175/JAS-D-12-0124.1.

——, S. Y. Matrosov, and N. B. Wood, 2016: Toward improving ice water content and snow-rate retrievals from radars. Part I: X and W bands, emphasizing *CloudSat*. *J. Appl. Meteor. Climatol.*, **55**, 2063–2090, doi:10.1175/JAMC-D-15-0290.1.

Hogan, R. J., and C. D. Westbrook, 2014: Equation for the microwave backscatter cross section of aggregate snowflakes using the self-similar Rayleigh–Gans approximation. *J. Atmos. Sci.*, **71**, 3292–3301, doi:10.1175/JAS-D-13-0347.1.

——, M. P. Mittermaier, and A. J. Illingworth, 2006: Retrieval of ice water content from radar reflectivity factor and temperature and its use in evaluating a mesoscale model. *J. Appl. Meteor. Climatol.*, **45**, 301–317, doi:10.1175/JAM2340.1.

——, L. Tian, P. R. Brown, C. D. Westbrook, A. J. Heymsfield, and J. Eastment, 2012: Radar scattering from ice aggregates using the horizontally aligned oblate spheroid approximation. *J. Appl. Meteor. Climatol.*, **51**, 655–671, doi:10.1175/JAMC-D-11-074.1.

Hou, A. Y., and Coauthors, 2014: The Global Precipitation Measurement mission. *Bull. Amer. Meteor. Soc.*, **95**, 701–722, doi:10.1175/BAMS-D-13-00164.1.

Korolev, A. V., and G. Isaac, 2003: Roundness and aspect ratio of particles in ice clouds. *J. Atmos. Sci.*, **60**, 1795–1808, doi:10.1175/1520-0469(2003)060<1795:RAAROP>2.0.CO;2.

Kosarev, A. L., and I. P. Mazin, 1991: An empirical model of the physical structure of upper-layer clouds. *Atmos. Res.*, **26**, 213–228, doi:10.1016/0169-8095(91)90055-2.

Leinonen, J., S. Kneiefel, D. Moisseev, J. Tyynela, S. Tanelli, and T. Nousiainen, 2012: Evidence of nonspheroidal behavior in millimeter-wavelength radar observations of snowfall. *J. Geophys. Res.*, **117**, D18205, doi:10.1029/2012JD017680.

Maahn, M., and U. Loehnert, 2017: Potential of higher-order moments and slopes of the radar Doppler spectrum for retrieving microphysical and kinematic properties of Arctic ice clouds. *J. Appl. Meteor. Climatol.*, **56**, 263–282, doi:10.1175/JAMC-D-16-0020.1.

Mather, J. H., and J. W. Voyles, 2013: The ARM Climate Research Facility: A review of structure and capabilities. *Bull. Amer. Meteor. Soc.*, **94**, 377–392, doi:10.1175/BAMS-D-11-00218.1.

Matrosov, S. Y., 1997: Variability of microphysical parameters in high-altitude ice clouds: Results of the remote sensing method. *J. Appl. Meteor.*, **36**, 633–648, doi:10.1175/1520-0450-36.6.633.

——, 2007: Modeling backscatter properties of snowfall at millimeter wavelengths. *J. Atmos. Sci.*, **64**, 1727–1736, doi:10.1175/JAS3904.1.

——, 2015: Evaluations of the spheroidal particle model for describing cloud radar depolarization ratios of ice hydrometeors. *J. Atmos. Oceanic Technol.*, **32**, 865–879, doi:10.1175/JTECH-D-14-00115.1.

——, and A. J. Heymsfield, 2008: Estimating ice content and extinction in precipitating cloud systems from *CloudSat* radar

measurements. *J. Geophys. Res.*, **113**, D00A05, doi:10.1029/2007JD009633.

——, ——, J. M. Intrieri, B. W. Orr, and J. B. Snider, 1995: Ground-based remote sensing of cloud particle sizes during the 26 November 1991 FIRE II cirrus case: Comparisons with in situ data. *Atmos. Sci.*, **52**, 4128–4142, doi:10.1175/1520-0469(1995)052<4128:GBRSOC>2.0.CO;2.

——, A. V. Korolev, and A. J. Heymsfield, 2002: Profiling cloud ice mass and particle characteristic size from Doppler radar measurements. *J. Atmos. Oceanic Technol.*, **19**, 1003–1018, doi:10.1175/1520-0426(2002)019<1003:PCIMAP>2.0.CO;2.

——, R. F. Reinking, and I. V. Djalalova, 2005: Inferring fall attitudes of pristine dendritic crystals from polarimetric radar data. *J. Atmos. Sci.*, **62**, 241–250, doi:10.1175/JAS-3356.1.

Protat, A. J., and Coauthors, 2016: The measured relationship between ice water content and cloud radar reflectivity in tropical convective clouds. *J. Appl. Meteor. Climatol.*, **55**, 1707–1729, doi:10.1175/JAMC-D-15-0248.1.

Shupe, M. D., J. M. Comstock, D. D. Turner, and G. G. Mace, 2016: Cloud property retrievals in the ARM program. *The Atmospheric Radiation Measurement (ARM) Program: The First 20 Years, Meteor. Monogr.*, No. 57, 19.1–19.20, doi:10.1175/AMSMONOGRAPHS-D-15-0030.1.

Skofronick-Jackson, G., and Coauthors, 2015: Global Precipitation Measurement Cold Season Precipitation Experiment (GCPEX): For measurement's sake, let it snow. *Bull. Amer. Meteor. Soc.*, **96**, 1719–1741, doi:10.1175/BAMS-D-13-00262.1.

Tanelli, S., S. L. Durden, E. Im, K. S. Pak, D. G. Reinke, P. Partain, J. M. Haynes, and R. T. Marchand, 2008: *CloudSat*'s cloud profiling radar after two years in orbit: Performance, calibration, and processing. *IEEE Trans. Geosci. Remote Sens.*, **46**, 3560–3573, doi:10.1109/TGRS.2008.2002030.